New Journal of Physics
The open access journal at the forefront of physics

Deutsche Physikalische Gesellschaft DPG IOP Institute of Physics

PAPER • OPEN ACCESS

Alternate attractor chimeralike states on rings of chaotic Lorenz-type oscillators

To cite this article: Hao Zhang *et al* 2024 *New J. Phys.* **26** 023016

IOP Publishing New J. Phys. 26 (2024) 023016 https://doi.org/10.1088/1367-2630/ad2411

New Journal of Physics
The open access journal at the forefront of physics

Deutsche Physikalische Gesellschaft DPG
IOP Institute of Physics

Published in partnership with: Deutsche Physikalische Gesellschaft and the Institute of Physics

OPEN ACCESS

RECEIVED
24 November 2023

REVISED
13 January 2024

ACCEPTED FOR PUBLICATION
30 January 2024

PUBLISHED
9 February 2024

PAPER

Alternate attractor chimeralike states on rings of chaotic Lorenz-type oscillators

Hao Zhang[1], **Zhili Chen**[1], **Fei Liu**[1], **Zhao Lei**[1,*], **Zhigang Zheng**[2,3,4,*] **and Yu Qian**[1,*]

[1] College of Physics and Optoelectronic Technology, Baoji University of Arts and Sciences, Baoji 721007, People's Republic of China
[2] Institute of Systems Science, Huaqiao University, Xiamen 361021, People's Republic of China
[3] College of Information Science and Engineering, Huaqiao University, Xiamen 361021, People's Republic of China
[4] School of Mathematical Sciences, Huaqiao University, Quanzhou 362021, People's Republic of China
[*] Authors to whom any correspondence should be addressed.

E-mail: leizhao1010@163.com, zgzheng@hqu.edu.cn and qianyu0272@163.com

Keywords: chimeralike state, Lorenz-type oscillator, chaotic collective behavior

Abstract

An interesting *alternate attractor chimeralike state* can self-organize to emerge on rings of chaotic Lorenz-type oscillators. The local dynamics of any two neighboring oscillators can spontaneously change from the chaotic butterfly-like attractors to the two symmetric and converse ones, which forms alternate attractors on the ring. This is distinctly different from the traditional chimera states with unique local attractor. An *effective driven-oscillator approach* is proposed to reveal the mechanism in forming this new oscillation mode and predict the critical coupling strengths for the emergence of the new oscillation mode. The existence of a pair of converse focus solutions with respect to the external drive is found to be the key factor responsible for the *alternate attractor chimeralike state*. The *linear feedback control scheme* is introduced to control the suppression and reproduction of *alternate attractor chimeralike state*. These findings may shed light on a new perspective of the studies and applications of chimera dynamics in complex systems.

1. Introduction

In the past few decades, exploring the collective behaviors in extended dynamical systems had attracted great attentions in the field of nonlinear science. Chimera state, which consists of coexisting coherent and incoherent subpopulations within an ensemble of coupled identical oscillators, is one of the most fascinating collective behaviors in this field [1–4]. This highly counter-intuitive structure was first reported by Kuramoto and Battogtokh in 2002 [5], in the symmetrically and nonlocally coupled system consisting of identical complex Ginzburg–Landau oscillators, and later termed as the 'chimera state' by Abrams and Strogatz due to its analogy to the Greek mythological creature made up of different animals [6]. Importantly, researchers have confirmed that chimera states that can self-organize to emerge in coupled identical oscillator systems are largely induced by the spontaneous breaking of spatial symmetry.

Early pioneering works aroused the tide of more theoretical and experimental contributions in this field, and extensive progresses on the issue of chimera states have been achieved. Experimentally, chimera states were successfully observed in optical analogs of coupled map lattices [7], populations of coupled Belousov–Zhabotinsky oscillators [8], mechanical oscillator networks [9], and time-delayed electronic circuits [10]. Theoretical studies claimed that the nonlocal coupling is the necessary condition for the formation of chimera states. Further investigations demonstrated that chimera or chimeralike states can also emerge in systems with purely local coupling [11], global coupling [12], adaptive coupling [13], time-varying coupling [14], hierarchical connectivities [15], and star structures [16], the single paradigmatic network models [17–19], such as small-world networks, Erdös–Rényi networks, and scale-free networks for typical examples, and even the multilayer networks [20]. Moreover, besides the initial coupled phase-oscillator systems, a variety of other systems with distinct local dynamics, such as time-delayed oscillators [21], discrete maps [22], continuous chaotic systems [23], limit-cycle elements [24], bursting neurons [25], bistable

models [26], quantum systems [27], and excitable units [28] were shown to perform chimera or chimeralike behaviors.

Recently, chimera or chimeralike states in neuronal networks have attracted great attentions, and rich interesting phenomena are reported [29–32]. For example, Wang *et al* found the chimeras in an adaptive neuronal network with burst-timing-dependent plasticity [29]. Hussain *et al* first identified the chimeras in a network of photosensitive FitzHugh–Nagumo neurons [30], and then discovered the chimera states in a multi-weighted neuronal network [32]. Furthermore, for practical applications, the robustness and control of chimera states are also important issues [33–38]. Omelchenko *et al* discussed the robustness of chimera states for coupled FitzHugh–Nagumo oscillators with perturbed threshold parameters [33]. Isele *et al* investigated the control of chimera states in oscillatory FitzHugh–Nagumo networks by introducing excitable units [34]. The lifetime of chimera states could be significantly enhanced by delayed couplings [36]. Controlling chimera states in chaotic oscillator ensembles through linear augmentation was studied by Khatun *et al* [38].

Chimera or chimeralike states may behave with various interesting spatiotemporal patterns. For example, breathing chimeras [39], spiral-wave chimeras [40], multi-chimeras [41], amplitude-mediated chimeras [42], chimeralike states [43], phase-flip chimeras [44], traveling chimeras [45], self-propelled chimeras [46], as well as frequency chimeras [47], have been identified in different kinds of complex systems. These findings can give us rich clues in understanding the mechanism of some physiological phenomena such as the unihemispheric sleep of some marine mammals [48] and the first-night effect in human sleep [49], and guiding the treatments of tumors [50] and epilepsy [51].

The formation and patterns of chimera states depend crucially on both the coupling strategy and local dynamics. Most of the previous studies of chimera or chimeralike states were focused on local dynamics with a single attractor. Very few investigations with respect to the chimera or chimeralike states composed of identical oscillators performing distinct local attractors have been reported. It is our motivation to seek for new types of chimera or chimeralike states that can self-organize to emerge in coupled oscillator systems with multiple local attractors. In this work, an *alternate attractor chimeralike state* (AACS) is exposed on rings of chaotic Lorenz-type oscillators. By introducing the *effective driven-oscillator approach*, the mechanism in forming the AACS on the rings is revealed, and the critical coupling strengths for the formation of the AACS are predicted. Moreover, the *linear feedback control scheme* is proposed to control the AACS and confirmed in numerical simulations.

The remainder of the paper is organized as follows. Section 2 studies the local dynamics of a single Lorenz-type oscillator. In section 3, the typical collective behaviors emerged on rings of chaotic Lorenz-type oscillators, i.e. the trivial chaotic behavior and the novel AACS, are extensively investigated. The mechanism discussion and further the control of AACS are carried out in sections 4 and 5, respectively. Section 6 reports other types of chimera states emerged on the Lorenz-type rings. Finally, we give the conclusion in section 7.

2. Multiple-attractor dynamics of a single Lorenz-type oscillator

The Lorenz-type oscillator was proposed by Yang and Wei in 2010 [52, 53], which is described by the following equations:

$$\begin{aligned}\frac{\mathrm{d}x}{\mathrm{d}t} &= a\left(y-x\right),\\ \frac{\mathrm{d}y}{\mathrm{d}t} &= -cy-xz,\\ \frac{\mathrm{d}z}{\mathrm{d}t} &= -b+xy.\end{aligned} \tag{1}$$

Here x, y, z are state variables, and a, b, c are dimensionless parameters. We fix $a = 10$ and $b = 100$, and the parameter c is adjusted in the region $[-20, 20]$ to investigate the local dynamics of a single oscillator. The above equations are numerically integrated by the fourth-order Runge-Kutta algorithm with the integral step $\triangle t = 0.001$, and random initial conditions are utilized.

Theoretically, we first analyze the Lorenz-type oscillator in terms of the linear stability analysis. A single Lorenz-type oscillator possesses two equilibria $E_1(\sqrt{b}, \sqrt{b}, -c)$ and $E_2(-\sqrt{b}, -\sqrt{b}, -c)$. The Jacobian derived from linear stability analysis of these two equilibria has the same eigenvalue equation as follows:

$$\lambda^3 + (a+c)\,\lambda^2 + b\lambda + 2ab = 0. \tag{2}$$

For the above parameter setting, two out of the three eigenvalues $\lambda_{1,2}$ are imaginary, while λ_3 is real number, implying that these two equilibria $E_{1,2}$ are foci.

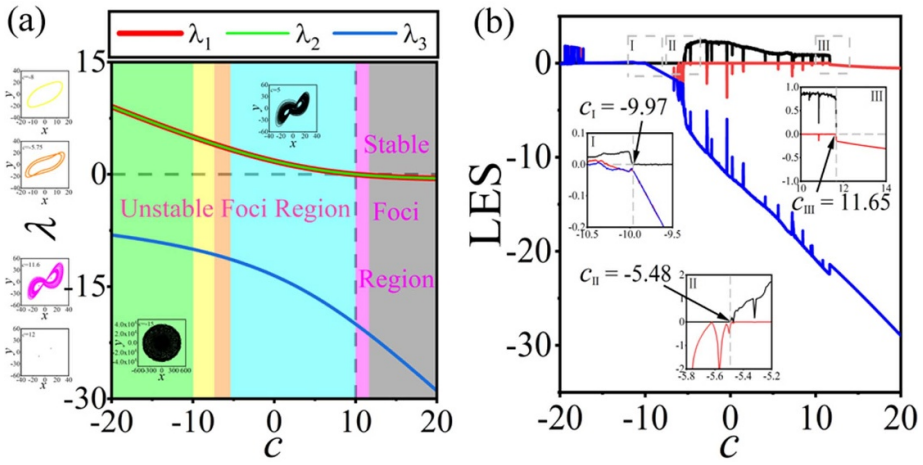

Figure 1. The theoretical and numerical analyses of the single Lorenz-type oscillator. (a) The dependence of the three eigenvalues of the linearized equation $\lambda_{1\sim3}$ on the system parameter c, and the colorful parameter regions for the six different kinds of local attractors. (b) The relationship between the Lyapunov exponent spectrum (LES) and the system parameter c. The three insets present the critical parameter regions where the local chaotic behaviors can emerge.

The stability of local focus solutions $E_{1,2}$ are shown in figure 1(a) by plotting the relationship between the three eigenvalues $\lambda_{1\sim3}$ and the parameter c. Only real parts of the two imaginary eigenvalues (λ_1 and λ_2, denoted by the red and green lines respectively) are plotted. When $\mathrm{Re}\lambda_{1\sim3} < 0$, $E_{1,2}$ are stable. Therefore the parameter plane c is divided into the unstable region (the left part in figure 1(a)) and the stable region (the right part), which are separated by the vertical dashed line located at $c = 10$.

Numerically, by varying parameter c in the region $[-20, 20]$, six different kinds of local dynamical behaviors of the single Lorenz-type oscillator can be observed and the corresponding local attractors are identified, i.e. the large-scale black chaotic trajectory for $c \in [-20, -9.97]$ (defined as the chaotic attractor and located in the light-green region in figure 1(a)), the single yellow periodic orbit for $c \in [-9.96, -7.35]$ (the monostable periodic attractor in the light-yellow region), the double orange periodic orbits for $c \in [-7.34, -5.49]$ (the bistable periodic attractor in the light-orange region), the black butterfly-like trajectory for $c \in [-5.48, 10]$ (the butterfly-like attractor in the light-blue region), the coexistence of the pink butterfly-like trajectory and the two pink points for $c \in [10.01, 11.65]$ (the bi-attractors in the light-pink region), and the purely two grey points for $c \in [11.66, 20]$ (the two-fixed-point attractor in the light-grey region), respectively. This indicates that a single Lorenz-type oscillator possesses diverse local attractors by modulating the parameter c.

To further confirm the local chaotic behaviors that can spontaneously emerge on the single Lorenz-type oscillator, the relationship between the Lyapunov exponent spectrum (LES) and the system parameter c within the above parameter regions is plotted, which is shown in figure 1(b). The three insets present the critical parameter regions where the local chaotic behaviors can emerge, which coincide well with the above three chaotic attractors observed in numerical simulations. Furthermore, we should also mention that, by plotting the dependence of the interspike interval on the parameter c (not shown here), the emergence route of chaos of the Lorenz-type oscillator model is revealed to be the period-doubling form.

Based on the theoretical and numerical results demonstrated in figure 1, we can find that, for a single Lorenz-type oscillator, the local unstable focus solutions can support different dynamical behaviors such as the chaotic attractor, the monostable and bistable periodic attractors, and the butterfly-like attractor (i.e. the left four parameter regions in figure 1(a)). As a comparison, the local stable foci can maintain the bi-attractors and the two-fixed-point attractor (i.e. the right two parameter regions). On the basis of these diverse dynamical behaviors of a single Lorenz-type oscillator, let us explore rich collective behaviors of coupled systems.

3. Trivial chaotic collective behavior and novel AACS emerged on the Lorenz-type rings

We focus on a ring consisting of $N = 100$ Lorenz-type oscillators, which is constructed with the nearest-neighbor couplings through variable x. This kind of coupling scheme is usually applied to study the

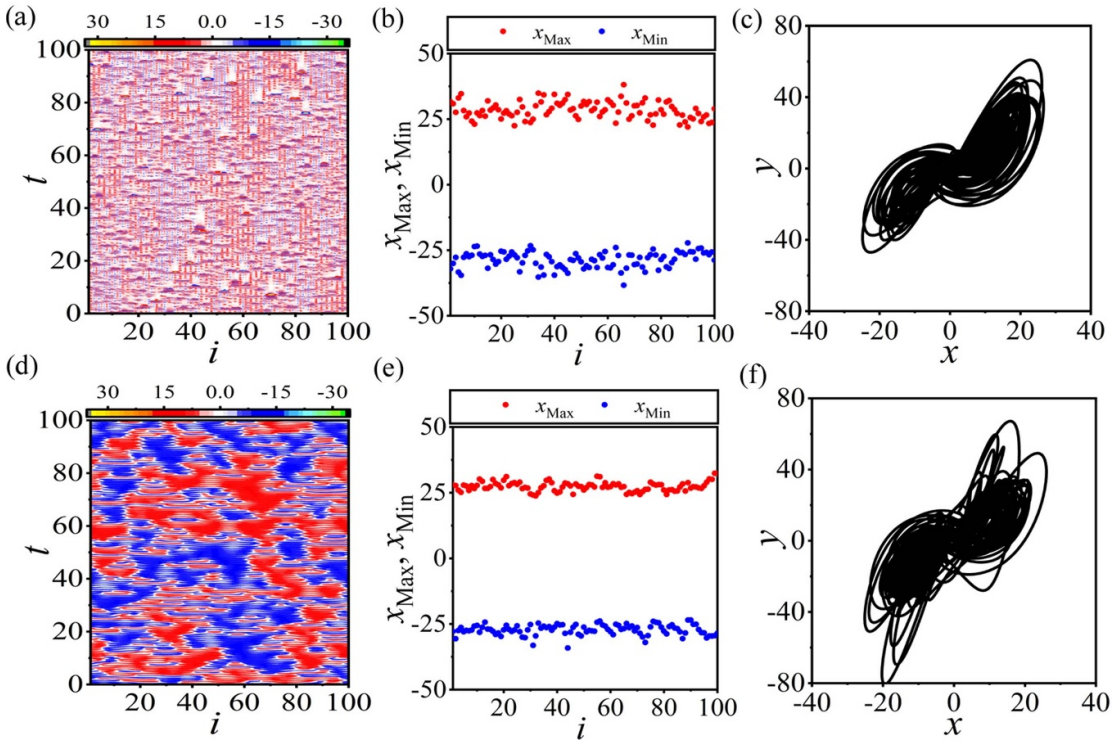

Figure 2. The trivial chaotic collective behaviors emerged on the Lorenz-type rings. The results obtained for different coupling strengths ε, i.e. a weaker coupling $\varepsilon = 5$ for the first row (a)–(c) and a stronger coupling $\varepsilon = 30$ for the second row (d)–(f). A chaotic parameter $c = 5$ located in the light-blue butterfly-like attractor region is selected for the local dynamics. The left, middle, and right columns are respectively the spatiotemporal patterns ((a) and (d)), the distributions of x_{Max} and x_{Min} of all elements on the rings ((b) and (e)), and the phase trajectories of the cell $i = 50$ ((c) and (f)).

chimera or chimeralike states in coupled oscillator systems [54–56]. The dynamics of the ring network of coupled Lorenz-type oscillators is governed by the following equations:

$$\begin{aligned}\frac{\mathrm{d}x_i}{\mathrm{d}t} &= a\left(y_i - x_i\right) + \varepsilon\left(x_{i+1} + x_{i-1} - 2x_i\right),\\ \frac{\mathrm{d}y_i}{\mathrm{d}t} &= -cy_i - x_i z_i,\\ \frac{\mathrm{d}z_i}{\mathrm{d}t} &= -b + x_i y_i.\end{aligned} \tag{3}$$

Here $i = 1, 2, \ldots, N$, and N is the length of ring. ε is the coupling strength between nearest linking oscillators. Periodic boundary condition $x_{i+N}(t) = x_i(t)$ is utilized in numerical simulations.

We first explore the dynamics for locally chaotic case by selecting $c = 5$ (located in the light-blue butterfly-like attractor region in figure 1(a)). Figure 2 shows the collective behaviors on the rings for different coupling strengths ε, where a weaker coupling $\varepsilon = 5$ for the first row (figures 2(a)–(c)) and a stronger coupling $\varepsilon = 30$ for the second row (figures 2(d)–(f)). The spatiotemporal patterns displayed in figures 2(a) and (d) (left column of figure 2) reveal that for both weak and strong couplings the collective behaviors emerged on the Lorenz-type rings are chaotic. To further demonstrate this behavior, we introduce two quantities as $x_{Max} = \mathrm{Max}\{x(t)\}$ and $x_{Min} = \mathrm{Min}\{x(t)\}$, where $\mathrm{Max}\{x(t)\}$ ($\mathrm{Min}\{x(t)\}$) are the maximum (minimum) values of the time series $x(t)$. These two quantities give the range of the phase trajectory along the x-axis direction and are effective indicators revealing the dynamical behavior (attractor property) of the local Lorenz-type oscillator. The two quantities x_{Max} and x_{Min} of all elements on the rings are plotted respectively in figures 2(b) and (e) (middle column of figure 2), where all values of x_{Max} (x_{Min}) are almost equal. This means that all oscillators on the rings can perform similar dynamical behaviors (or we can say have similar attractors). Figures 2(c) and (f) (right column of figure 2) expose the phase trajectories of the cell $i = 50$ on the rings, where a local oscillator for both weak and strong couplings perform chaotic butterfly-like behaviors, which are similar to the butterfly-like attractor obtained for a single Lorenz-type oscillator shown in figure 1(a). So a trivial chaotic behavior can self-organize to emerge on the Lorenz-type rings with local chaotic dynamics. Here we should mention that similar spatiotemporal chaos patterns can also be observed in coupled logistic lattices [57].

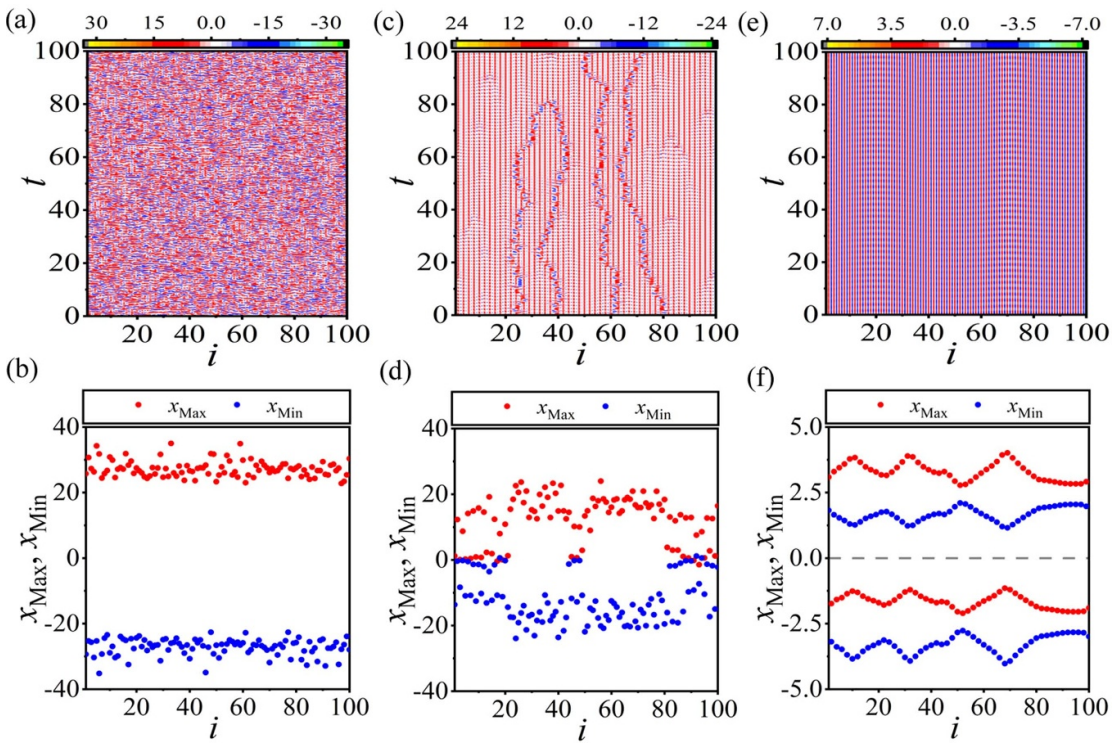

Figure 3. The transition from the trivial chaotic collective behavior to the novel *alternate attractor chimeralike state* (AACS) emerged on the Lorenz-type rings. Another neighboring local chaos parameter $c = -5$ located in the light-blue butterfly-like attractor region is selected for the local dynamics. The first and the second rows respectively display the spatiotemporal patterns ((a), (c), (e)) and the distributions of x_{Max} and x_{Min} of all elements on the rings ((b), (d), (f)) for three different coupling strengths, i.e. $\varepsilon = 5$ for the left column ((a) and (b), the chaotic behavior with a weak coupling), $\varepsilon = 15$ for the middle column ((c) and (d), the mixed state with a moderate coupling), and $\varepsilon = 30$ for the right column ((e) and (f), the AACS with a strong coupling).

It is crucial to study whether other kinds of collective behaviors can be obtained with local chaotic dynamics. To do this, we study the collective behavior for another neighboring local chaos parameter $c = -5$ (also in the light-blue butterfly-like attractor region in figure 1(a)), with which a single Lorenz-type oscillator still performs a chaotic butterfly-like motion. Figures 3(a) and (b) (left column of figure 3) respectively show the spatiotemporal pattern and the distribution of x_{Max} and x_{Min} for a weaker coupling $\varepsilon = 5$. A similar trivial chaotic collective behavior to figure 2 can be observed on the ring. To check the property of the local attractor, the phase trajectory of the element $i = 50$ is plotted in figure 4(a), where a similar butterfly-like attractor to figure 2 is found.

However, situation changes dramatically as the coupling strength is further increased. Figure 3(c) shows the spatiotemporal pattern of the Lorenz-type ring at a moderate coupling $\varepsilon = 15$. It can be found that the global dynamics consists of two coexisting dynamical modes, in which some of oscillators execute chaotic evolutions, while the others perform regular oscillations. We call this state as the mixed state. The distribution of x_{Max} and x_{Min} of all elements on the ring is drawn in figure 3(d). Most of these two quantities are still found to be located around the values $x_{\mathrm{Max}} \approx 20$ and $x_{\mathrm{Min}} \approx -20$, respectively indicating a large-scale chaotic motion of local oscillators. It is interesting that the motion of some oscillators can perform regular oscillation restricted in a small phase space.

When the coupling strength further increases, as shown in figure 3(e), a distinctly new spatiotemporal pattern can be observed. For example, for a stronger coupling $\varepsilon = 30$, the alternative colored red and blue stripes are clearly exposed. This means that any two neighboring oscillators in the ring can perform regular oscillations with completely different amplitudes. One can further observe the distribution of x_{Max} and x_{Min} in figure 3(f). The horizontal gray dashed line located at $x = 0$ is the boundary between the two converse domains with a positive region ($x > 0$) and a negative region ($x < 0$). If both x^i_{Max} and x^i_{Min} of the ith oscillator locate in the positive region, its neighbor oscillators $i \pm 1$ must be in the conversely negative region, and vice versa. This implies that any two neighboring oscillators in the ring can perform regular oscillations in the symmetric and converse regions of the phase space, which consequently possess alternate attractors. We call the oscillation mode in figures 3(e) and (f) as the *alternate attractor chimeralike state*.

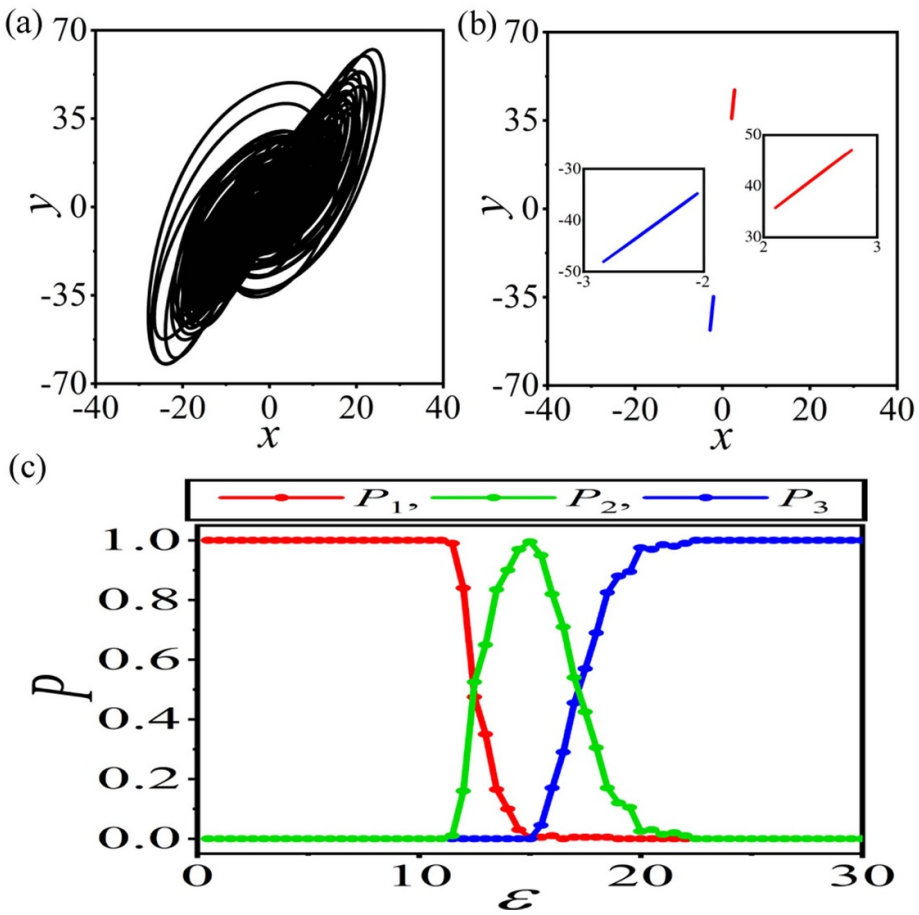

Figure 4. The local attractors of the chaotic collective behavior and the AACS, and the corresponding transitions. (a) The phase trajectory of the element $i = 50$ corresponding to the chaotic collective behavior shown in figures 3(a) and (b). (b) The similar phase trajectories of the two conversely neighboring elements $i = 50$ (red lines) and $i = 51$ (blue lines) corresponding to the AACS shown in figures 3(e) and (f). The two insets show the local amplifications. (c) The dependence of the probabilities of chaotic behavior (red dot line), mixed state (green dot line), and AACS (blue dot line) on the coupling strength ε.

The phase trajectories of the two conversely neighboring elements $i = 50$ (red lines) and $i = 51$ (blue lines) are plotted in figure 4(b) to visually expose the local attractors of the AACS. The two insets show the local amplifications. It is revealed that the attractors of the local oscillators on the ring change dramatically from a chaotic butterfly-like attractor to two symmetric and converse ones. The emergence of AACS on the Lorenz-type ring is a typical collective behavior, which to our knowledge has not been systematically studied.

Although the alternate behaviors revealed in the AACS are similar to the results reported by Maistrenko *et al* [58], there exist two major differences. First, the mechanisms of these two kinds of alternate behaviors are different. In [58], the alternate behaviors in the antiphase chimera state are caused by the existence of a reverse phase difference in the coherent two elements. For the case we reported here, the existence of two symmetric and converse local attractors is the key factor. Second, the sub-populations that can perform alternate behaviors in these two cases are different. In the case of antiphase chimera state emerged on the ring containing three oscillators, only two coherent elements can implement alternate behaviors. In our case, any two neighboring oscillators on the ring can execute alternate behaviors.

It is necessary to discuss the transition from chaotic behavior to AACS emerged on the Lorenz-type rings. The dependence of the probabilities of chaotic behavior (red dot line), mixed state (green dot line), and AACS (blue dot line) on the coupling strength ε are plotted in figure 4(c), where two transitions are revealed. It is exposed that as ε increases, the first transition from chaotic behavior to mixed state happens. When the coupling strength is further increased, the transition from mixed state to AACS emerges. This interprets why AACS can only self-organize to emerge on rings of chaotic Lorenz-type oscillators at strong couplings. Based on the results exposed in figure 4(c), the transition from chaotic behavior to AACS on the Lorenz-type rings is revealed explicitly.

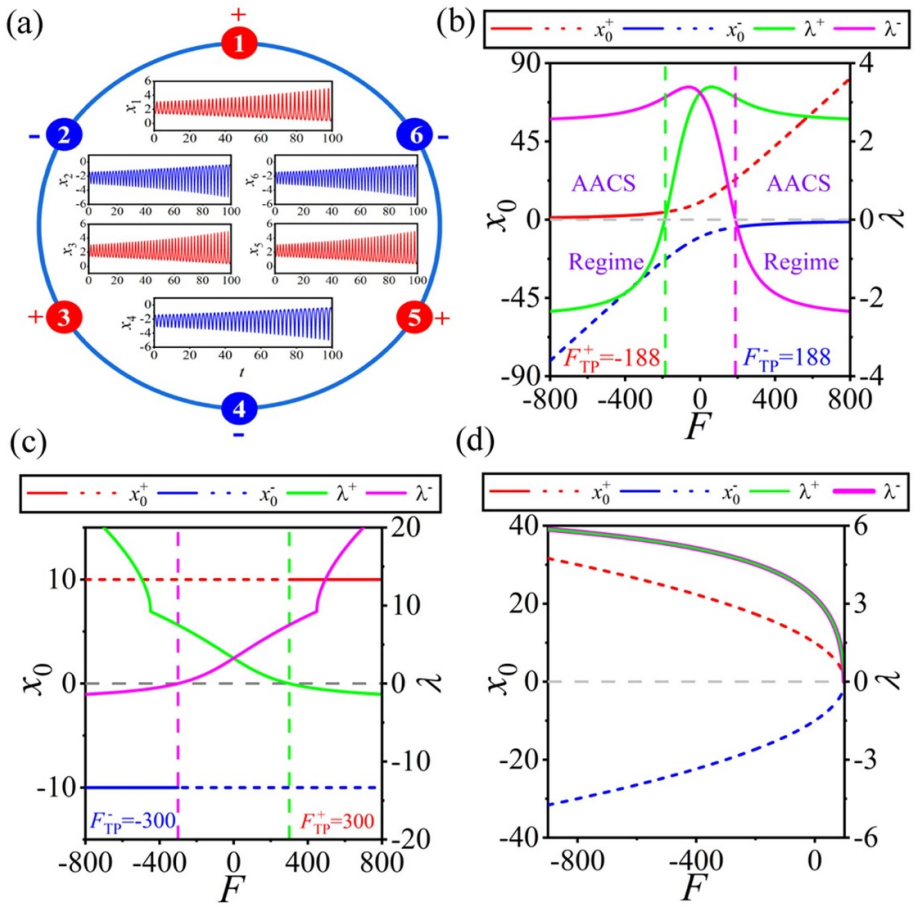

Figure 5. The mechanism discussion of AACS based on the *effective driven-oscillator approach*. (a) A simplified model of a ring containing $N = 6$ chaotic Lorenz-type oscillators. The time series of the variable x for each oscillator started from random initial condition is also demonstrated. The oscillators in the positive region are symbolled by '+' and are colored in red, while the negative ones are denoted by '−' and blue. (b) The dependence of the two local foci $x_0{}^{+}$ and $x_0{}^{-}$ (respectively denoted by the red and blue lines, belonging to the left axis) of the driven-oscillator model and their determinant eigenvalues λ^{+} and λ^{-} (respectively indicated by the green and pink lines, belonging to the right axis) on the external drive F. The solid red and blue lines indicate that $x_0{}^{+}$ and $x_0{}^{-}$ are stable, while the dashed ones mean the unstable foci. The green and pink dashed lines instruct the two critical driving forces (or we can say the two boundaries), outside of which the stable oscillation mode of AACS can self-organize to emerge on the rings. (c), (d) Similar theoretical analyses obtained by the *effective driven-oscillator approach* for the y variable coupling (c) and the z variable coupling (d). Here the external drives F in (c) and (d) respectively present the equivalent external drives acting on the target oscillator by the nearest-neighbor couplings through variables y and z.

4. Mechanism discussion of AACS

It is important to understand the mechanism why the oscillation mode of AACS can self-organize to emerge on the Lorenz-type rings with chaotic local dynamics. To explore this issue, a simplified model of a ring containing $N = 6$ chaotic Lorenz-type oscillators is constructed, which is illustrated in figure 5(a). The time series of the component $x(t)$ for each oscillator started from a random initial condition is also demonstrated. It is shown that $N = 6$ chaotic oscillators are spontaneously divided into a positive group (the oscillators with variable $x > 0$) and a negative group (the oscillators with variable $x < 0$), which are symbolled by '+' and '−', and are colored in red and blue, respectively. Alternatively, for an oscillator, one may consider the couplings from its nearest converse neighbors as an equivalent external drive. Therefore an *effective driven-oscillator approach* is proposed to reveal the mechanism in forming the AACS on the Lorenz-type rings, which is described by the following equations:

$$\begin{aligned}\frac{\mathrm{d}x}{\mathrm{d}t} &= a\,(y - x) + F,\\ \frac{\mathrm{d}y}{\mathrm{d}t} &= -cy - xz,\\ \frac{\mathrm{d}z}{\mathrm{d}t} &= -b + xy.\end{aligned} \tag{4}$$

Here F represents the equivalent external drive acting on the target oscillator by nearest-neighbor couplings through variable x.

Similarly, by applying the linear stability analysis, the above driven-oscillator model still has two focus solutions. As we consider only the x-axis direction, two local foci are respectively symbolled by ${x_0}^+$ (corresponding to the positive focus) and ${x_0}^-$ (to the negative one), and their stabilities are determined by the corresponding determinant eigenvalues λ^+ (corresponding to the focus ${x_0}^+$) and λ^- (to the ${x_0}^-$). Figure 5(b) presents the dependence of two local foci ${x_0}^+$ and ${x_0}^-$ (respectively denoted by the red and blue lines, belonging to the left axis) of the driven-oscillator model and their determinant eigenvalues λ^+ and λ^- (respectively indicated by the green and pink lines, belonging to the right axis) on the external drive F. The solid red and blue lines indicate that ${x_0}^+$ and ${x_0}^-$ are stable, while the dashed ones mean the unstable foci, which are determined by the corresponding determinant eigenvalues.

Here we use the positive focus solution ${x_0}^+$ (red solid and dashed lines) to give further discussions. It is shown in figure 5(b) that the corresponding eigenvalue λ^+ (green line) varies dramatically as the external drive F changes, which consequently affects the stability of the local focus ${x_0}^+$. Specifically, as the external drive $F>0$, the eigenvalue $\lambda^+>0$. This means that a positive focus solution ${x_0}^+$ in this non-converse driving region (i.e. $F>0$) is unstable. However, when the external drive decreases into the negative region (i.e. $F<0$) and is less than a threshold (instructed by the green dashed line), the eigenvalue λ^+ changes from $\lambda^+>0$ to $\lambda^+<0$. This implies that the stability of the corresponding local focus ${x_0}^+$ transits from unstable to stable simultaneously. A stable positive focus solution ${x_0}^+$ can be obtained for the conversely negative external drive. Similar stability transition can also happen to the local focus ${x_0}^-$, and the stable negative focus solution ${x_0}^-$ can be obtained for the conversely positive external drive. Furthermore, the two critical driving forces (or we can say the two boundaries), at which the corresponding converse local foci can change from unstable to stable, are given by the intersection points of the eigenvalue curves and the gray dashed threshold line located at $x=0$, and are instructed by the green (${F^+}_{\rm TP}=-188$, corresponding to the conversely positive focus ${x_0}^+$) and pink (${F^-}_{\rm TP}=188$, to the ${x_0}^-$) dashed lines, respectively. In the regions outside of these two dashed boundaries (i.e. the left region from the green dashed line and the right region from the pink dashed line), the driven-oscillator model has a conversely stable focus solution and a non-conversely unstable one, which are the key factors in forming the AACS on the rings. So these regions are named as the AACS regimes, which are exposed in figure 5(b) explicitly.

Based on the above discussions, the mechanism why the AACS can self-organize to emerge on the Lorenz-type rings can be explained. We use the positive oscillators (symbolled by '+' and colored in red) shown in figure 5(a) as the example to address this issue. It is shown that each positive Lorenz-type oscillator is driven by two conversely negative neighbors. These neighboring drivings will be amplified by the coupling strength. When the coupling strength exceeds a certain critical value, all the equivalent external drives now can fall into the AACS regime, which consequently make the corresponding positive oscillators stable in this situation. Similarly, the conversely external drives from positive neighbors will help the negative oscillators become stable. Therefore, after a short transient, the Lorenz-type oscillators started from random initial conditions can spontaneously perform alternately converse dynamical behaviors, and the stable collective behavior of AACS can self-organize to emerge on the rings.

The *effective driven-oscillator approach* can also be applied to predict whether the new oscillation mode of AACS can self-organize to emerge on the Lorenz-type rings with other forms of couplings. Figures 5(c) and (d) expose the similar theoretical analyses obtained for the y variable coupling (figure 5(c)) and the z variable coupling (figure 5(d)), in which the external drives F in figures 5(c) and (d) respectively present the equivalent external drives acting on the target oscillator by the nearest-neighbor couplings through variables y and z. It is revealed explicitly that, the key factor in forming the AACS, i.e. the existence of a pair of converse focus solutions with respect to the external drive, has not been found both in these two cases. Specifically, for the y variable coupling (i.e. figure 5(c)), there exists a pair of non-converse focus solutions with respect to the external drive. While for the z variable coupling (i.e. figure 5(d)), the two solutions in the entire external drive region are all unstable. Based on these theoretical analyses, we can predict that the new oscillation mode of AACS can not self-organize to emerge on the Lorenz-type rings with the nearest-neighbor couplings through variables y and z. Importantly, these predictions have been confirmed in numerical simulations.

Remarkably, the critical coupling strength in forming the AACS on the Lorenz-type rings can also be approximately predicted based on the *effective driven-oscillator approach*. Here we use the ith oscillator on the schematic network shown in figure 5(a) as an example. Because the nearest-neighbor coupling scheme as equation (3) is adopted in the ring structure, the equivalent external drive of the ith oscillator paced from its two converse neighbors $i+1$ and $i-1$ can be written as:

$$F_i=\varepsilon\left(x_{i+1}+x_{i-1}-2x_i\right). \tag{5}$$

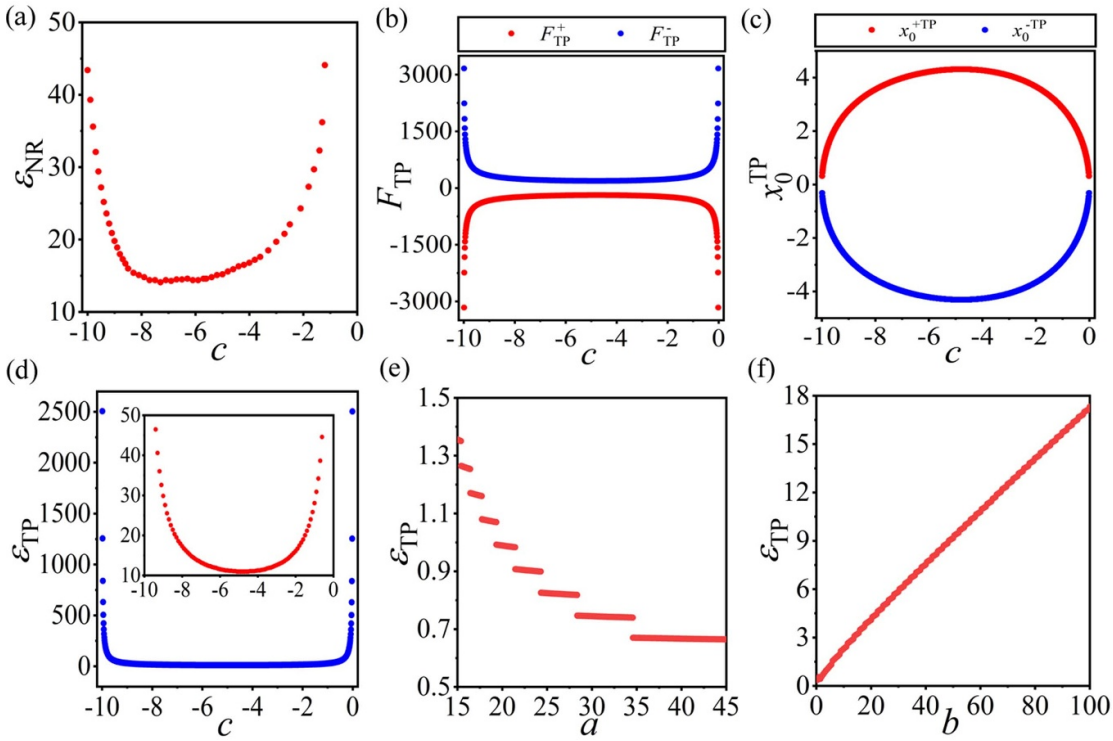

Figure 6. The numerical and theoretical studies of the critical coupling strength in forming the AACS on the Lorenz-type rings. (a) The numerical critical coupling strengths ε_{NR} obtained for different parameters c. (b)–(d) The theoretical predictions of the critical pacing strengths $F^{+}{}_{TP}$ and $F^{-}{}_{TP}$ (b), the critical local foci ${x_0}^{+TP}$ and ${x_0}^{-TP}$ (c), and the critical coupling strengths ε_{TP} (d) forecasted by the *effective driven-oscillator approach* for different parameters c. The inset in (d) is the corresponding local amplification, which coincides well with the numerical results ε_{NR} shown in (a). (e), (f) Similar theoretical predictions obtained for other parameters a (e) and b (f).

As stated above, if and only if these equivalent external drives for each oscillators reach the critical values $F^{\pm}{}_{TP}$ ($F^{+}{}_{TP}$ for the positive oscillators and $F^{-}{}_{TP}$ for the negative ones), the local oscillators can perform conversely stable foci ${x_0}^{+TP}$ and ${x_0}^{-TP}$, based on which the stable AACS can self-organize to emerge on the rings. In the process of theoretical prediction, the equivalent external drives $F^{\pm}{}_{TP}$ can be predicted by the eigenvalue analysis discussed above, and ${x_0}^{\pm TP}$ are the critical focus solutions of the driven-oscillator model obtained at $F^{\pm}{}_{TP}$. By substituting $F^{\pm}{}_{TP}$ and ${x_0}^{\pm TP}$ into equation (5), one can approximately obtain the following two symmetric equations:

$$F^{\pm}{}_{TP} \approx \varepsilon_{TP}\left({x_0}^{\mp TP} + {x_0}^{\mp TP} - 2{x_0}^{\pm TP}\right), \tag{6}$$

based on which the critical coupling strength in forming the AACS on the rings can be approximately derived as:

$$\varepsilon_{TP} \approx \frac{|F_{TP}|}{4\,|{x_0}^{TP}|}. \tag{7}$$

To verify the validity of the above theoretical prediction, the numerical results of the critical coupling strength ε_{NR} in forming the AACS on the rings containing $N = 100$ Lorenz-type oscillators for different parameters c are studied, which are revealed in figure 6(a). It is shown that the numerical critical coupling strength ε_{NR} initially decreases as the parameter c increases, and then passes through a minimum value, and finally increases, implying that an optimal parameter may facilitate the emergence of AACS on the rings. According to the above analysis, the critical pacing strengths $F^{+}{}_{TP}$ and $F^{-}{}_{TP}$, and the critical local foci ${x_0}^{+TP}$ and ${x_0}^{-TP}$ can be predicted, as shown in figures 6(b) and (c), respectively. Based on these results and the formula presented in equation (7), the critical coupling strengths ε_{TP} in forming the AACS forecasted by the *effective driven-oscillator approach* for different parameters c are unveiled in figure 6(d). The corresponding local amplification shown in the inset of figure 6(d) coincides well with the numerical results ε_{NR} shown in figure 6(a). This confirms the validity of this new analysis method we proposed here. Furthermore, similar theoretical predictions for other parameters a and b are also tested, which are presented in figures 6(e) and (f), respectively. All the results revealed in figure 6 can definitely prove that the AACS phenomena and

the *effective driven-oscillator approach* reported in the present paper are universal, which are irrelevant of system parameters.

5. Control of AACS on the Lorenz-type rings

The above analysis on the mechanism indicates that, the existence of a pair of converse focus solutions in the driven-oscillator model is the key factor in forming the stable collective behaviors of AACS on the rings. Here the property of 'converse' means that the stabilities of these two foci are converse to the external drive. Specifically, for the negative external drive, the positive focus solution is stable, while the negative one is unstable simultaneously, and vice versa. This gives us an inspiration that, the 'converse' property of these two focus solutions would change dramatically as the local dynamics of the driven-oscillator model is regulated. This is also valid for regulating the collective behaviors emerged on the rings, and possible control schemes (i.e. suppression and reproduction) of AACS may be realized.

To address this issue, we introduce a *linear feedback control scheme*. Specifically, a linear control term is applied to the variable y both in the driven-oscillator model of equation (4) and the corresponding Lorenz-type ring of equation (3), which now can be respectively described by the following equations:

$$\begin{aligned}\frac{\mathrm{d}x}{\mathrm{d}t} &= a\left(y-x\right)+F,\\ \frac{\mathrm{d}y}{\mathrm{d}t} &= -cy-xz+ky,\\ \frac{\mathrm{d}z}{\mathrm{d}t} &= -b+xy,\end{aligned} \tag{8}$$

and

$$\begin{aligned}\frac{\mathrm{d}x_i}{\mathrm{d}t} &= a\left(y_i-x_i\right)+\varepsilon\left(x_{i+1}+x_{i-1}-2x_i\right),\\ \frac{\mathrm{d}y_i}{\mathrm{d}t} &= -cy_i-x_iz_i+ky_i,\\ \frac{\mathrm{d}z_i}{\mathrm{d}t} &= -b+x_iy_i.\end{aligned} \tag{9}$$

Here ky is the linear feedback term, and k is the control parameter. By varying the control parameter k, the effectively controllable region (i.e. the stable AACS regime) where the two converse focus solutions can emerge in the driven-oscillator model will change drastically, based on which the control of the collective behaviors of AACS on the Lorenz-type rings becomes available.

5.1. Suppression of AACS

Let us first investigate the suppression of AACS on the Lorenz-type rings. We choose $c=-5$, where the stable AACS can self-organize to emerge on a Lorenz-type ring, as shown in figure 3. By applying the *linear feedback control scheme* and varying the control parameter, the converse foci regions of the driven-oscillator model will change dramatically, and this also consequently impacts the collective behaviors on the rings. To ensure the effectiveness of the control scheme, a large external drive $F=-1000$ is utilized in the driven-oscillator model, and similar results can also be obtained for the symmetric external drive $F=1000$. The corresponding control performance is shown in figure 7(a), where the dependence of the two local foci ${x_0}^+$ and ${x_0}^-$ of the driven-oscillator model with $F=-1000$ and their corresponding determinant eigenvalues λ^+ and λ^- on the control parameter k are plotted. The stable focus solutions are drawn by the solid red and blue lines, while the unstable ones are denoted by the dashed lines, which are determined according to the corresponding eigenvalues. The two purple dashed lines guide the two boundaries (the lower threshold (LT) $k_{\mathrm{LT}}=-4.9$ and the upper threshold (UT) $k_{\mathrm{UT}}=4.9$), between which the conversely positive focus solution is stable (red solid line) and the non-conversely negative one is unstable (blue dashed line). This means that, if the control parameter k is selected within this parameter region, such as the example shown in figure 3 with $k=0$ (i.e. without control), a stable AACS is expected to emerge on the Lorenz-type rings. So we call this region as the AACS regime. However, when k locates beyond the AACS regime, the oscillation mode of AACS cannot self-organize to emerge on the rings, and one eventually achieves a suppression of AACS.

Figures 7(b)–(d) present the control results obtained on the Lorenz-type ring with the control parameter $k=-7.5$ outside of the AACS regime and the strong coupling $\varepsilon=30$, among which are the spatiotemporal pattern (figure 7(b)), the distribution of x_{Max} and x_{Min} of all elements on the ring (figure 7(c)), and the phase trajectory of the element $i=50$ (figure 7(d)). It is shown explicitly that, as the *linear feedback control scheme*

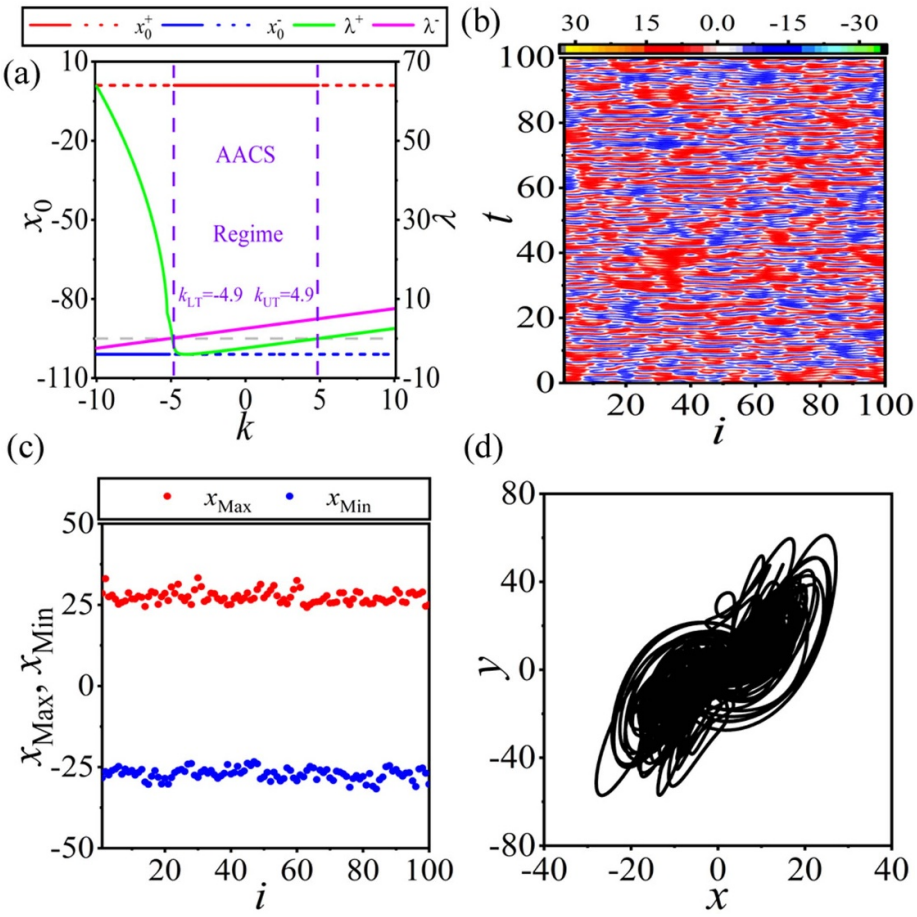

Figure 7. The suppression of AACS on the Lorenz-type rings. The system parameter $c = -5$ is selected as the example, with which the stable AACS can self-organize to emerge on a Lorenz-type ring without control as shown in figure 3. (a) The dependence of the two local foci $x_0{}^+$ and $x_0{}^-$ of the driven-oscillator model with the external driving force $F = -1000$ and their corresponding determinant eigenvalues λ^+ and λ^- on the control parameter k. The two purple dashed lines guide the two boundaries (the lower threshold (LT) $k_{LT} = -4.9$ and the upper threshold (UT) $k_{UT} = 4.9$), between which the stable AACS can self-organize to emerge on the rings. (b)–(d) The control results obtained on the Lorenz-type ring with the control parameter $k = -7.5$ (located outside of the AACS regime) and the strong coupling $\varepsilon = 30$: The spatiotemporal pattern (b), the distribution of x_{Max} and x_{Min} of all elements on the ring (c), and the phase trajectory of the element $i = 50$ (d).

is applied for the control parameter locating outside of the AACS regime, the initially stable oscillation mode of AACS is suppressed, and the trivial chaotic collective behavior will emerge on the ring. This well confirms the effectiveness of the *linear feedback control scheme* we proposed here.

5.2. Reproduction of AACS

Let us further attempt the reproduction of AACS on the Lorenz-type rings. The system parameter $c = 5$ is selected as the example. Figure 8(a) reveals the similar control performance predicted by the driven-oscillator model as figure 7(a). The stable AACS regime is indicated between the two purple dashed boundaries respectively located at $k_{LT} = 5.1$ and $k_{UT} = 14.9$. It is shown that for the control-free case (i.e. $k = 0$, which is located outside of the AACS regime), the trivial chaotic collective behaviors would emerge on the Lorenz-type rings, see figure 2 as an example. However, as the *linear feedback control scheme* is applied, by choosing an appropriate control parameter located in the AACS regime, the AACS on the Lorenz-type rings will be recovered.

Figures 8(b)–(d) demonstrate the control results on the Lorenz-type ring with $k = 10$ (located in the AACS regime) and a strong coupling $\varepsilon = 30$, where the spatiotemporal pattern (figure 8(b)), the distribution of x_{Max} and x_{Min} of all elements on the ring (figure 8(c)), and the phase trajectories of the two conversely neighboring elements $i = 50$ (red lines) and $i = 51$ (blue lines) and their local amplifications (figure 8(d)) are presented, respectively. The initially trivial chaotic collective behavior is controlled to the stable oscillation mode of the novel AACS. This further verifies the significance of the *effective driven-oscillator approach* proposed in this paper.

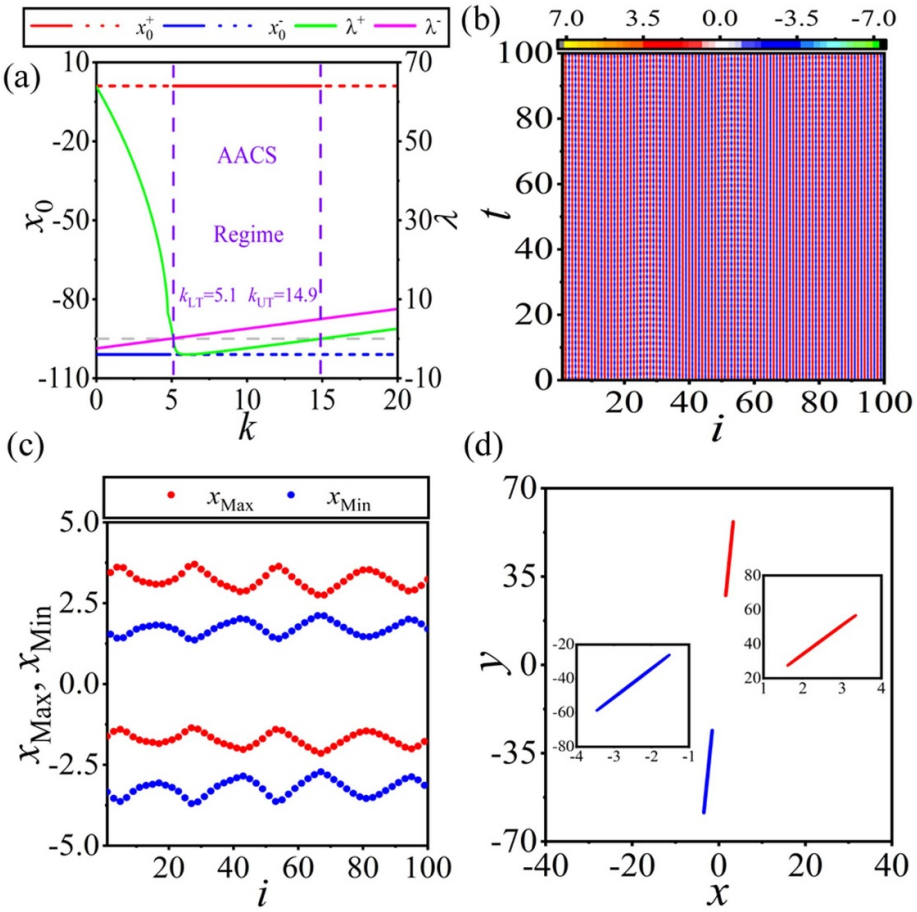

Figure 8. The reproduction of AACS on the Lorenz-type rings. (a) The similar control performance as figure 7(a) with the system parameter $c = 5$, based on which the Lorenz-type rings would perform chaotic behaviors without control as shown in figure 2. The stable AACS regime is indicated between the two purple dashed boundaries respectively located at $k_{LT} = 5.1$ and $k_{UT} = 14.9$. (b)–(d) The control results obtained on the Lorenz-type ring with the control parameter $k = 10$ (located in the AACS regime) and the strong coupling $\varepsilon = 30$: The spatiotemporal pattern (b), the distribution of x_{Max} and x_{Min} of all elements on the ring (c), and the phase trajectories of the two conversely neighboring elements $i = 50$ (red lines) and $i = 51$ (blue lines) and their local amplifications (d).

6. Other types of Chimera states emerged on the Lorenz-type rings

Besides the AACS, it is also interesting to seek for other types of chimera states that can self-organize to emerge on the Lorenz-type rings. Here we use the parameter located in light-pink bi-attractors region in figure 1(a) as an example to explore this issue. Figures 9(a)–(d) display the results obtained for the system parameter $c = 11.6$ with a weaker coupling $\varepsilon = 5$ for the mode shown in the first row and a stronger coupling $\varepsilon = 30$ for the second row.

It is shown in figure 9(a) that for the weaker coupling $\varepsilon = 5$ the spatiotemporal pattern exhibits three different colored regions composed of a pure red part, a pure blue part, and a narrowly alternately colored domain between these two pure parts, which respectively correspond to the large equilibrium state, the small equilibrium state, and the chaotic behavior. This coincides well with the coexisting dynamics of the butterfly-like trajectory and the two fixed points of the single Lorenz-type oscillator. We call this interesting three coexisting mode state as a multi-state chimera. The distribution of x_{Max} and x_{Min} of all elements on the ring shown in figure 9(b) further confirms the emergence of the multi-state chimera on the Lorenz-type rings.

A stronger coupling $\varepsilon = 30$ will drastically change the situation. Instead of the multi-state chimera, a traveling chimera state shown by the spatiotemporal pattern in figure 9(c) can be observed. Figure 9(d) gives the corresponding distribution of x_{Max} and x_{Min}, which explicitly demonstrates the stable propagation of this chimera mode.

To further disclose the transition from the multi-state chimera to the traveling chimera on the Lorenz-type rings, we plot the dependence of the probabilities of multi-state chimera (red dot line), homogeneous equilibrium states (green dot line, containing homogeneous large equilibrium state and

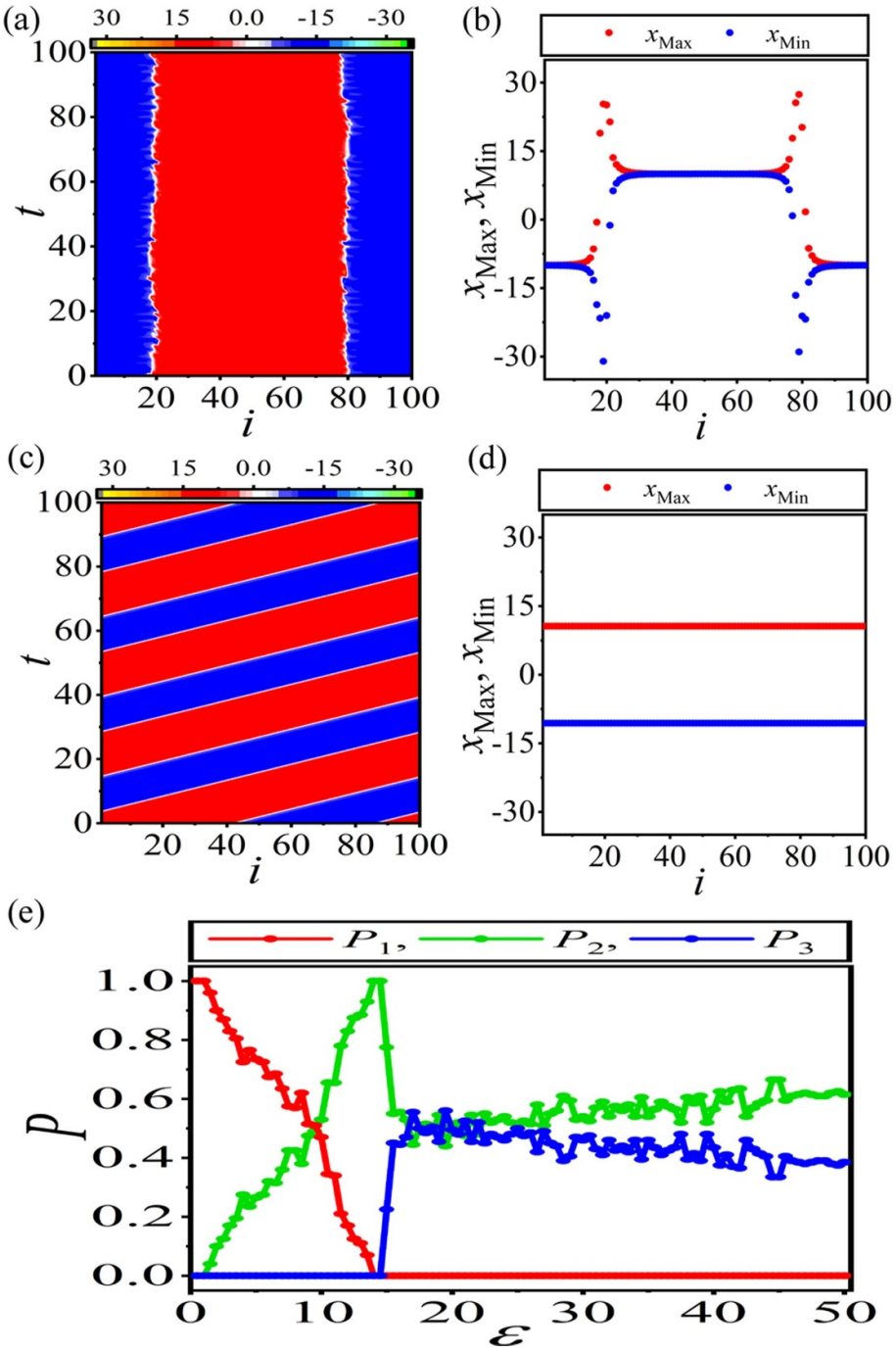

Figure 9. Other typical types of chimera states emerged on the Lorenz-type rings and the corresponding transitions. The multi-state chimera ((a) and (b)) and the traveling chimera ((c) and (d)) states self-organized to emerge on the Lorenz-type rings for the system parameter $c = 11.6$, with which the single Lorenz-type oscillator can perform coexisting local dynamics of the butterfly-like trajectory and the two fixed points (i.e. the light-pink bi-attractors region in figure 1(a)). The coupling strengths for the multi-state chimera and the traveling chimera are $\varepsilon = 5$ and $\varepsilon = 30$, respectively. (a) and (c) are the spatiotemporal patterns; (b) and (d) are the distributions of x_{Max} and x_{Min} of all elements on the rings. (e) The dependence of the probabilities of multi-state chimera (red dot line), homogeneous equilibrium states (green dot line), and traveling chimera (blue dot line) on the coupling strength ε.

homogeneous small equilibrium state), and traveling chimera (blue dot line) on the coupling strength ε in figure 9(e). Same as the transition from a chaotic behavior to the AACS emerged on the Lorenz-type rings (see figure 4(c)), similar transitions can also be found for the current case. It is revealed that as the coupling strength ε increases, the first transition from the multi-state chimera to the homogeneous equilibrium state occurs. When the coupling strength is further increased, a traveling chimera starts to emerge and coexists with the homogeneous equilibrium state, which constitutes the second transition. We can conclude from figure 9 that the multi-state chimera and the traveling chimera states can self-organize to emerge on the

Lorenz-type rings for the coexisting local dynamics of the butterfly-like trajectory and the two fixed points. The transition between these two chimera states is exposed explicitly.

7. Conclusion

To summarize, abundant collective behaviors that can self-organize to emerge on the Lorenz-type rings have been extensively investigated. To do this, the local dynamics of a single Lorenz-type oscillator is first studied. Theoretical and numerical analyses of the single Lorenz-type oscillator reveal six different kinds of local dynamical behaviors, including the chaotic attractor, the monostable periodic attractor, the bistable periodic attractor, the butterfly-like attractor, the bi-attractors, and the two-fixed-point attractor.

When Lorenz-type oscillators with local butterfly-like attractor are coupled with a ring topology, besides the trivial collective disordered behaviors, an interesting oscillation mode is observed. It is revealed that the local dynamical behaviors of any two neighboring oscillators can spontaneously change from the chaotic butterfly-like attractors to the two symmetric and converse ones. This can form *alternate attractor chimeralike state*, which is definitely different from the traditional chimera states with unique local attractor. This new type of oscillation mode, to our knowledge, has not been studied in detail till now. The transition from the chaotic behavior to the AACS is also disclosed.

By introducing an equivalent external drive acting on the target oscillator, which represents the two drivings from its nearest converse neighbors, an *effective driven-oscillator approach* is proposed to theoretically understand the mechanism in forming the AACS on the rings. In terms of linear stability analysis, a pair of converse focus solutions with respect to the external drive is confirmed to be the key factor in forming the stable oscillation mode of AACS. Importantly, the critical coupling strengths in forming the AACS on the Lorenz-type rings with different system parameters are also predicted by this approach, which coincide well with numerical results. We have also confirmed that both the AACS phenomena and the *effective driven-oscillator approach* proposed in the present paper are universal, which are irrelevant of system parameters.

Furthermore the *effective driven-oscillator approach* inspires us to consider a successful control of AACS on the Lorenz-type rings. By introducing the *linear feedback control scheme* to the driven-oscillator model, the control strategy is predicted by the eigenvalue analysis, and the controllable AACS regimes are revealed explicitly, based on which the suppression and the reproduction of AACS on the corresponding controlled Lorenz-type rings can be successfully achieved. Besides the AACS, we have also explored other potential collective states that can self-organize to emerge on the Lorenz-type rings. The multi-state chimera and the traveling chimera states are observed, which possess coexisting local dynamics of the butterfly-like trajectory and the two fixed points. The transition between these two chimera states is also uncovered clearly.

The traditional chimera state, which has rigorously coherent and incoherent domains, is an interesting and important issue and has been extensively investigated in the last two decades since it was first reported by Kuramoto and Battogtokh in nonlocally coupled oscillator systems with perfectly symmetric structure and identical system parameters. However, in real-world complex systems, such as neuronal networks, brain systems, power networks, and social systems, the network structures may not be strictly symmetric and the local dynamics may not be homogeneous. In these cases, instead of the traditional chimera state, complex chimera patterns can be observed, which may not possess rigorously coherent and incoherent regions. These kinds of complex chimera patterns are usually called chimeralike states [19, 20, 43, 54] or generalized chimeras [56]. We believe extensive explorations of the formation, the mechanism, the control, and the application of complex chimera patterns in different kinds of complex systems will become hot topics in the interdisciplinary fields of complexity science and life science due to potential and extensive applications. The *alternate attractor chimeralike states* and the corresponding *effective driven-oscillator approach* reported here may shed light on a new perspective in explorations of these intriguing patterns.

Data availability statement

The data that support the findings of this study will be openly available following an embargo at the following URL/DOI: https://coderzhanghao.gitee.io/.

Acknowledgments

This work is supported by the National Natural Science Foundation of China (Grant Nos. 12375031, 12375033), the Natural Science Basic Research Plan in Shaanxi Province of China (Grant Nos. 2022JZ-03, 2022GD-TSLD-27, 2024SF-YBXM-134), the Shaanxi Fundamental Science Research Project for

Mathematics and Physics (Grant No. 22JSY021), the Baoji University of Arts and Sciences Innovative Research Project of Postgraduates (Grant Nos. YJSCX23YB34, YJSCX22ZD02), and the Youth Innovation Team of Shaanxi Universities.

ORCID iD

Zhigang Zheng https://orcid.org/0000-0002-1421-0442

References

[1] Yao N and Zheng Z 2016 Chimera states in spatiotemporal systems: theory and applications *Int. J. Mod. Phys.* B **30** 1630002
[2] Majhi S, Bera B K, Ghosh D and Perc M 2019 Chimera states in neuronal networks: a review *Phys. Life Rev.* **28** 100
[3] Wang Z and Liu Z 2020 A brief review of chimera state in empirical brain networks *Front. Physiol.* **11** 724
[4] Parastesh F, Jafari S, Azarnoush H, Shahriari Z, Wang Z, Boccaletti S and Perc M 2021 Chimeras *Phys. Rep.* **898** 1
[5] Kuramoto Y and Battogtokh D 2002 Coexistence of coherence and incoherence in nonlocally coupled phase oscillators *Nonlinear Phenom. Complex Syst.* **5** 380
[6] Abrams D M and Strogatz S H 2004 Chimera states for coupled oscillators *Phys. Rev. Lett.* **93** 174102
[7] Hagerstrom A M, Murphy T E, Roy R, Hövel P, Omelchenko I and Schöll E 2012 Experimental observation of chimeras in coupled-map lattices *Nat. Phys.* **8** 658
[8] Tinsley M R, Nkomo S and Showalter K 2012 Chimera and phase-cluster states in populations of coupled chemical oscillators *Nat. Phys.* **8** 662
[9] Martens E A, Thutupalli S, Fourrière A and Hallatschek O 2013 Chimera states in mechanical oscillator networks *Proc. Natl Acad. Sci. USA* **110** 10563
[10] Larger L, Penkovsky B and Maistrenko Y 2013 Virtual chimera states for delayed-feedback systems *Phys. Rev. Lett.* **111** 054103
[11] Laing C R 2015 Chimeras in networks with purely local coupling *Phys. Rev.* E **92** 050904(R)
[12] Hart J D, Bansal K, Murphy T E and Roy R 2016 Experimental observation of chimera and cluster states in a minimal globally coupled network *Chaos* **26** 094801
[13] Chandrasekar V K, Sheeba J H, Subash B, Lakshmanan M and Kurths J 2014 Adaptive coupling induced multi-stable states in complex networks *Physica* D **267** 36
[14] Buscarino A, Frasca M, Gambuzza L V and Hövel P 2015 Chimera states in time-varying complex networks *Phys. Rev.* E **91** 022817
[15] Ulonska S, Omelchenko I, Zakharova A and Schöll E 2016 Chimera states in networks of Van der Pol oscillators with hierarchical connectivities *Chaos* **26** 094825
[16] Meena C, Murali K and Sinha S 2016 Chimera states in star networks *Int. J. Bifurcation Chaos* **26** 1630023
[17] Zhu Y, Zheng Z and Yang J 2014 Chimera states on complex networks *Phys. Rev.* E **89** 022914
[18] Andreev A V, Frolov N S, Pisarchik A N and Hramov A E 2019 Chimera state in complex networks of bistable Hodgkin–Huxley neurons *Phys. Rev.* E **100** 022224
[19] Lei Z, Zhang C, Wang Y, Wei Z, Qian Y and Zheng Z 2023 Chimeralike oscillation modes in excitable scale-free networks *Phys. Rev. Res.* **5** 013006
[20] Frolov N S, Maksimenko V A, Makarov V V, Kirsanov D V, Hramov A E and Kurths J 2018 Macroscopic chimeralike behavior in a multiplex network *Phys. Rev.* E **98** 022320
[21] Sethia G C, Sen A and Atay F M 2008 Clustered chimera states in delay-coupled oscillator systems *Phys. Rev. Lett.* **100** 144102
[22] Omelchenko I, Maistrenko Y, Hövel P and Schöll E 2011 Loss of coherence in dynamical networks: spatial chaos and chimera states *Phys. Rev. Lett.* **106** 234102
[23] Omelchenko I, Riemenschneider B, Hövel P, Maistrenko Y and Schöll E 2012 Transition from spatial coherence to incoherence in coupled chaotic systems *Phys. Rev.* E **85** 026212
[24] Omelchenko I, Omel'chenko O E, Hövel P and Schöll E 2013 When nonlocal coupling between oscillators becomes stronger: patched synchrony or multichimera states *Phys. Rev. Lett.* **110** 224101
[25] Bera B K, Ghosh D and Lakshmanan M 2016 Chimera states in bursting neurons *Phys. Rev.* E **93** 012205
[26] Shepelev I A, Vadivasova T E, Bukh A V, Strelkova G I and Anishchenko V S 2017 New type of chimera structures in a ring of bistable FitzHugh–Nagumo oscillators with nonlocal interaction *Phys. Lett.* A **381** 1398
[27] Xu H, Wang G, Huang L and Lai Y 2018 Chaos in dirac electron optics: emergence of a relativistic quantum chimera *Phys. Rev. Lett.* **120** 124101
[28] Lei Z, Pu S, Zhang H, Yao C, Qian Y and Zheng Z 2022 Bistability-induced chimeras in one-dimensional paced excitable rings with nonlocal couplings *Europhys. Lett.* **139** 62001
[29] Wang Z, Baruni S, Parastesh F, Jafari S, Ghosh D, Perc M and Hussain I 2020 Chimeras in an adaptive neuronal network with burst-timing-dependent plasticity *Neurocomputing* **406** 117
[30] Hussain I, Jafari S, Ghosh D and Perc M 2021 Synchronization and chimeras in a network of photosensitive FitzHugh–Nagumo neurons *Nonlinear Dyn.* **104** 2711
[31] Simo G R, Njougouo T, Aristides R P, Louodop P, Tchitnga R and Cerdeira H A 2021 Chimera states in a neuronal network under the action of an electric field *Phys. Rev.* E **103** 062304
[32] Hussain I, Jafari S, Perc M and Ghosh D 2022 Chimera states in a multi-weighted neuronal network *Phys. Lett.* A **424** 127847
[33] Omelchenko I, Provata A, Hizanidis J, Schöll E and Hövel P 2015 Robustness of chimera states for coupled FitzHugh–Nagumo oscillators *Phys. Rev.* E **91** 022917
[34] Isele T, Hizanidis J, Provata A and Hövel P 2016 Controlling chimera states: the influence of excitable units *Phys. Rev.* E **93** 022217
[35] Ujjwal S R, Punetha N, Prasad A and Ramaswamy R 2017 Emergence of chimeras through induced multistability *Phys. Rev.* E **95** 032203
[36] Gjurchinovski A, Schöll E and Zakharova A 2017 Control of amplitude chimeras by time delay in oscillator networks *Phys. Rev.* E **95** 042218
[37] Omelchenko I, Hülser T, Zakharova A and Schöll E 2019 Control of chimera states in multilayer networks *Front. Appl. Math. Stat.* **4** 67

[38] Khatun A A, Jafri H H and Punetha N 2021 Controlling chimera states in chaotic oscillator ensembles through linear augmentation *Phys. Rev.* E **103** 042202
[39] Abrams D M, Mirollo R, Strogatz S H and Wiley D A 2008 Solvable model for chimera states of coupled oscillators *Phys. Rev. Lett.* **101** 084103
[40] Martens E A, Laing C R and Strogatz S H 2010 Solvable model of spiral wave chimeras *Phys. Rev. Lett.* **104** 044101
[41] Ujjwal S R and Ramaswamy R 2013 Chimeras with multiple coherent regions *Phys. Rev.* E **88** 032902
[42] Sethia G C, Sen A and Johnston G L 2013 Amplitude-mediated chimera states *Phys. Rev.* E **88** 042917
[43] Dutta P S and Banerjee T 2015 Spatial coexistence of synchronized oscillation and death: a chimeralike state *Phys. Rev.* E **92** 042919
[44] Chandrasekar V K, Gopal R, Senthilkumar D V and Lakshmanan M 2016 Phase-flip chimera induced by environmental nonlocal coupling *Phys. Rev.* E **94** 012208
[45] Bera B K, Ghosh D and Banerjee T 2016 Imperfect traveling chimera states induced by local synaptic gradient coupling *Phys. Rev.* E **94** 012215
[46] Kruk N, Maistrenko Y and Koeppl H 2018 Self-propelled chimeras *Phys. Rev.* E **98** 032219
[47] Kachhara S and Ambika G 2021 Frequency chimera state induced by differing dynamical timescales *Phys. Rev.* E **104** 064214
[48] Mascetti G G 2016 Unihemispheric sleep and asymmetrical sleep: behavioral, neurophysiological and functional perspectives *Nat. Sci. Sleep* **8** 221
[49] Tamaki M, Bang J W, Watanabe T and Sasaki Y 2016 Night watch in one brain hemisphere during sleep associated with the first-night effect in humans *Curr. Biol.* **26** 1
[50] Koulierakis I, Verganelakis D A, Omelchenko I, Zakharova A, Schöll E and Provata A 2020 Structural anomalies in brain networks induce dynamical pacemaker effects *Chaos* **30** 113137
[51] Gerster M, Berner R, Sawicki J, Zakharova A, Skoch A, Hlinka J, Lehnertz K and Schöll E 2020 FitzHugh–Nagumo oscillators on complex networks mimic epileptic-seizure-related synchronization phenomena *Chaos* **30** 123130
[52] Yang Q, Wei Z and Chen G 2010 An unusual 3D autonomous quadratic chaotic system with two stable node-foci *Int. J. Bifurcation Chaos* **20** 1061
[53] Wei Z and Yang Q 2010 Anti-control of Hopf bifurcation in the new chaotic system with two stable node-foci *Appl. Math. Comput.* **217** 422
[54] Clerc M G, Ferré M A, Coulibaly S, Rojas R G and Tlidi M 2017 Chimera-like states in an array of coupled-waveguide resonators *Opt. Lett.* **42** 2906
[55] Clerc M G, Coulibaly S, Ferré M A and Rojas R G 2018 Chimera states in a Duffing oscillators chain coupled to nearest neighbors *Chaos* **28** 083126
[56] Clerc M G, Coulibaly S and Ferré M A 2020 Freak chimera states in a locally coupled Duffing oscillators chain *Commun. Nonlinear Sci. Numer. Simul.* **89** 105288
[57] Kaneko K 1989 Spatiotemporal chaos in one-and two-dimensional coupled map lattices *Physica* D **37** 60
[58] Maistrenko Y, Brezetsky S, Jaros P, Levchenko R and Kapitaniak T 2017 Smallest chimera states *Phys. Rev.* E **95** 010203(R)